Int. J. Heat Mass Transfer. Vol. 29, No. 10, pp. 1553–1563, 1986
Printed in Great Britain

0017-9310/86 $3.00+0.00
Pergamon Journals Ltd.

Heat transfer and pressure drop characteristics of an array of plates aligned at angles to the flow in a rectangular duct

Y. N. LEE

Borg-Warner Corporation, Roy C. Ingersoll Research Center, Wolf & Algonquin Roads, Des Plaines, IL 60018, U.S.A.

(*Received* 3 *September* 1985 *and in final form* 1 *May* 1986)

Abstract—The heat transfer and pressure drop characteristics of an array of plates, aligned at various angles of $\theta = 20$–$35°$ to the direction of air flow in a rectangular, straight duct, have been investigated experimentally in the range of Reynolds numbers between 350 and 5000. The heat transfer coefficients of the forward and back sides of the plates have been separately determined, and the average coefficient between the two closely approximates the laminar short duct theory at low Reynolds numbers ($N_{Re,Dh} \leqslant 1200$) and is nearly independent of the angle of alignment with respect to the air flow direction. However, at higher Reynolds number ($N_{Re,Dh} \geqslant 1500$) the average coefficient deviates significantly from the theory. The pressure drop measurements through the plate array showed that the streamwise, per-row coefficient K_p is a function of only the plate angle and independent of the Reynolds number $N_{Re,Dh}$.

INTRODUCTION

FLOW INTERRUPTION created in flow passages at periodic intervals is a popular means for heat transfer enhancement in compact heat exchangers. Slit fins used for various industrial compact heat exchangers and louvered fins for automotive radiators are examples. The slit fin provides a means of boundary-layer control. Namely, new velocity and thermal boundary layers develop over each fin segment created by the slit; since the developing boundary-layer flow is characterized by higher heat transfer coefficients than a fully developed flow, performance enhancement is obtained. The louvered fin attempts further enhancement by inclining the segments against the fluid flow to create turbulence and vorticity. Since, however, any thermal improvement is normally accompanied by a pressure drop increase, an optimum balance between the two must be sought.

There are numerous publications in which the effectiveness of the aforementioned augmentation was investigated. In most cases measurements were made of the average heat transfer coefficient through wind-tunnel tests of actual heat exchangers [1–6]. Although useful, this approach does not provide detailed information on the fundamental processes occurring within the heat exchanger. However, a fundamental investigation of slit fin augmentation recently appeared in the literature [7–9]. In the latter study, the heat transfer and pressure drop characteristics of an array of colinear and staggered plates aligned parallel to the flow direction were investigated. The present work encompasses studies of an array of plates aligned at angles to the fluid flow. The heat transfer and pressure drop characteristics of an array of three lanes (see Fig. 2), each lane consisting of eight plates, in a straight duct ($W = 196.6$ mm $\times$ $H = 91.5$ mm), were experimentally determined. The plates were aligned at angles of 20°, 25°, 30° and 35° to the flow direction.

In contrast to plates aligned parallel to the air flow [7–9], the heat transfer coefficients of the two sides of a plate in the present study (the forward side and the back side) are expected to be different. To determine separately the two heat transfer coefficients is, however, very difficult using conventional heat transfer measurement techniques. Therefore, a technique based on the analogy between mass and heat transfer processes [10] has been utilized. From the analogy, the convective mass transfer coefficient can be converted into the convective heat transfer coefficient. A total of three plate lanes were used for the experiments, among which the test plate lane was located in the middle between the two other so-called 'dummy lanes'. The dummy lanes were there simply to satisfy the fluid dynamic boundary conditions. The test plates were all identical and each plate was made of metal substrate (stainless-steel, 0.400 mm thick), one side of which was coated with a layer of naphthalene 0.514 mm thick; the overall thickness, t, of the test plate (metal substrate and naphthalene coating) was 0.914 mm. The dummy plates were made of stainless-steel 0.914 mm thick. The flow length of all plates was fixed at $L_p = 21.5$ mm; thus the thickness to flow length ratio was fixed at $t/L_p = 0.0425$. The lane pitch was fixed at $H_p = 30.5$ mm; thus the lane pitch to flow length ratio was $H_p/L_p = 1.419$, which resulted in the aspect ratio α [$= W/(H_p - t)$] being fixed at 6.64. The forward-side heat transfer coefficient of the plates was determined separately from the back-side coefficient, and an average value of the flow was taken as the average heat transfer coefficient. In addition to the heat transfer studies, pressure drop through the

NOMENCLATURE

A total surface area for flow [m^2]
A_c minimum cross-sectional flow area [m^2]
A_m total active mass (heat) transfer area [m^2]
Dh hydraulic diameter of plate array defined by equation (4) [mm]
D hydraulic diameter of duct [mm]
$\mathscr{D}$ diffusion coefficient [$m^2\,h^{-1}$]
H duct height [mm]
H_p plate lane pitch [mm]
h heat transfer coefficient [kcal $h^{-1}\,m^{-1}\,°C^{-1}$]
h_m mass transfer coefficient [m h^{-1}]
k thermal conductivity [kcal $h^{-1}\,m^{-1}\,°C^{-1}$]
K_c pressure loss coefficient defined by equation (11) [—]
$(K_c)_{max}$ maximum K_c [—]
K_p pressure coefficient per row defined by equation (10) [—]
L total length of array, NL_p [m]
L_p plate length in flow direction [mm]
L_D duct length corresponding to one plate length [m]
M total mass sublimated during a time period [kg]
n power to Prandtl number and Schmidt number [—]
N number of plates per lane [—]
$N_{Nu,Dh}$ Nusselt number based on Dh defined by equation (3)′ [—]
$(N_{Nu,Dh})$ Nusselt number of continuous duct [—]
N_{Pr} Prandtl number of air [—]
$N_{Re,Dh}$ Reynolds number based on Dh defined by equation (5) [—]
N_{Sc} Schmidt number [—]
$N_{Sh,Dh}$ Sherwood number based on Dh defined by equation (3) [—]
$N_{St,Dh}$ Stanton number for heat transfer defined by equation (6)′ [—]
$(N_{St,Dh})_m$ Stanton number for mass transfer defined by equation (6) [—]
P pressure [mmHg]
P_{Baro} barometric pressure [mmHg]
ΔP_N net pressure drop of array [$N\,m^{-2}$]
ΔP_T total pressure drop [$N\,m^{-2}$]
ΔP_f pressure drop due to friction [$N\,m^{-2}$]
ΔP_p pressure drop due to plate array [$N\,m^{-2}$]
ΔP_e entrance/exit losses [$N\,m^{-2}$]
PP pumping power [m^2]
St Stanton number, $N_{Sh,Dh}/N_{Re,Dh}N_{Sc}$ or $N_{Nu,Dh}/N_{Re,Dh}N_{Pr}$ [—]
t plate thickness [mm]
V_{max} average flow velocity through A_c [m h^{-1}]
V average approaching velocity [m h^{-1}]
W duct width [mm]
X distance from duct inlet [cm].

Greek symbols

α aspect ratio = $W/(H_p - t)$ for plate array or continuous duct [—]
θ plate (or louver) angle with respect to flow [deg]
μ viscosity of air [kg $h^{-1}\,m^{-1}$]
ρ density of air [kg m^{-3}]
$\Delta\rho_m$ log mean concentration difference defined by equation (2) [kg m^{-3}]
ρ_{ne} naphthalene vapor concentration at exit of test section [kg m^{-3}]
ρ_{nw} naphthalene vapor concentration at the plate surface [kg m^{-3}]
ν kinematic viscosity of air [$m^2\,h^{-1}$]
τ time [h]
ρ_{no} naphthalene concentration at entrance of test section [kg m^{-3}].

array was measured to determine the net and the overall pressure drop with the identical values of t/L_p and H_p/L_p to those of the heat transfer array but in a scaled-down duct (3.6:1).

Preliminary tests were conducted to examine the variation of the mass transfer coefficient of individual plates. It was found that the coefficients were identical except that the first plate had a slightly higher coefficient. Therefore, all experiments were conducted with eight plates except that a limited number of tests were conducted with the entire array to confirm the accuracy of the data.

The net pressure drop is the net internal pressure drop through the plate array. The total pressure drop, on the other hand, is the sum of the net pressure drop and the pressure drop which manifests in the external vicinity of the last plate. This external pressure drop is recoverable as the flow progresses downstream along the duct.

EXPERIMENTAL APPARATUS AND PROCEDURES

The main features of the test rig are shown schematically in Fig. 1.

The test system has two air flow systems, one for test air and one for controlling test air temperature. The part of the system designated as the test air system is outlined with heavy lines in Fig. 1.

In operation, air from the supply box (9) is induced through test section (1) by the blower (2), or by the

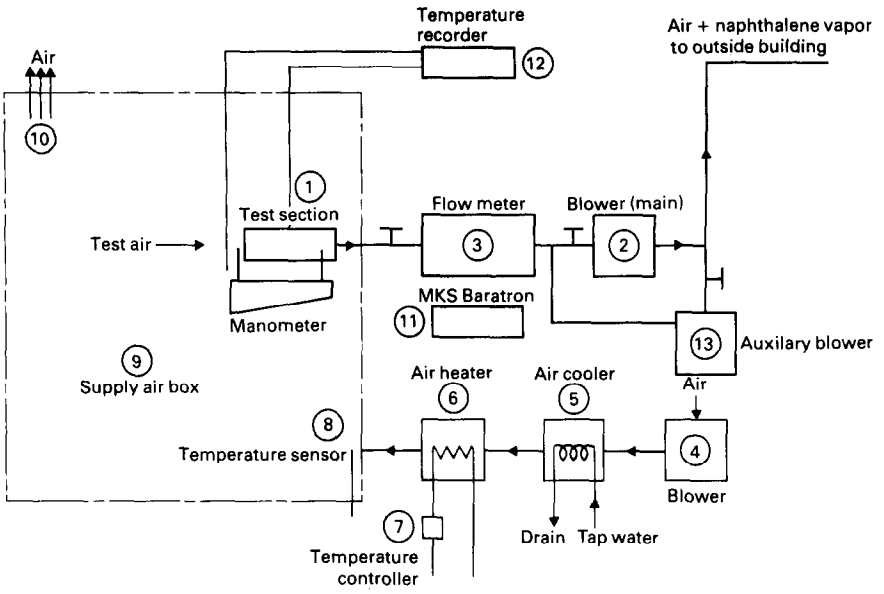

FIG. 1. Schematic diagram of experimental setup.

auxiliary blower. From the test section, this air (plus naphthalene vapor) flows successively through the flow meter (3) containing a series of ASME flow nozzles, the blower (2), and exit piping to the exterior of the laboratory.

The pressure drops across the flow nozzles are monitored by a manometer or a pressure transducer (11) (range, 0–1 mmHg). Temperatures of the test air and the naphthalene test model are measured with copper–constantan thermocouples connected to a temperature recorder (12).

The naphthalene concentration at the surface of the model enters into the computation of the mass transfer coefficient and this concentration depends on the surface temperature of the model. Since a given model must be tested for a considerable time interval ($\sim$ 15–90 min) to obtain an accurately measurable weight loss, it follows that both the air and model temperature must be closely controlled.

The portion of the system bounded by fine lines in Fig. 1 is designed to hold the test section, the model and the test air at a constant temperature, independent of laboratory temperature excursions. In operation, the blower (4) draws air from the laboratory and forces it through a water-cooled coil (5). This cooled air is then reheated to the desired test section temperature by an electrical heater (6) which is powered by a temperature controller (7) whose thermistor sensor (8) is located at the inlet to the supply air box (9). The bulk of this conditioned air flows through the thermally insulated supply air box and dumps back into the laboratory through opening (10). Supply box (9) is specifically designed to keep the through-flow velocity low while insuring good mixing within the box. Only a small fraction of the box air is drawn through the test section. Temperatures within the supply box are readily held within ± 0.1°C of setpoint temperature, usually 25°C.

Test section for mass transfer tests

The test section and its dimensions are shown in Fig. 2. It consists of three parts: the upper, the middle and the lower. The upper part is made of two sides and a top plate, all Plexiglas. The two sides have slots to receive 'dummy' plates. The lower part is similar to the upper, except that it has the bottom plate instead of the top plate. The middle part has only two sides, which have slots for receiving the test plates.

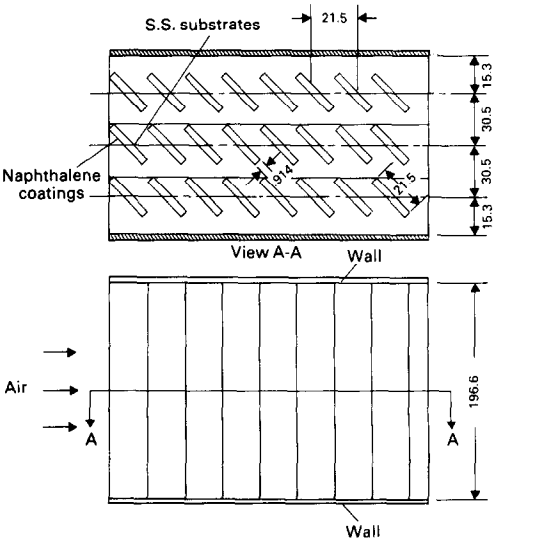

Units of measure are in mm.

FIG. 2. Sketch of mass transfer test section.

As indicated earlier, only the plates in the middle lane need naphthalene coating in the main part of the present work. The coating is machined so that the total thickness of the naphthalene and the metal substrate is equal to the thickness of the metal plates in the upper and the lower lanes.

Test section for pressure drop tests

The test section built for pressure drop is shown in Fig. 3. It consists of three segments: the inlet, the test section and the exit. The segment for the test section is similar to that of the mass transfer test section, except that the size is now 3.6 times smaller than the mass transfer test section. The inlet duct is 38.1 cm long and the exit duct is 20.5 cm long. Extension of the duct is made to measure pressure drop at the entrance and near the exit of the test section.

Test plate preparation for mass transfer tests and experimental procedure

In order to coat naphthalene on the metal substrate (0.400 mm thick) and machine the naphthalene coating to a 0.514 mm thickness (total thickness 0.914 mm), special equipment is necessary. The main component of this equipment is a hollow, rectangular, shallow box [Fig. 4(a)]. Its top and bottom faces are machined and the top has numerous holes. The box has a connection to the vacuum pump. When the metal plates are placed side by side on the top face so as to cover all the holes, the box is connected to the vacuum pump and the metal plates adhere to the platform (top face) under vacuum action through the holes.

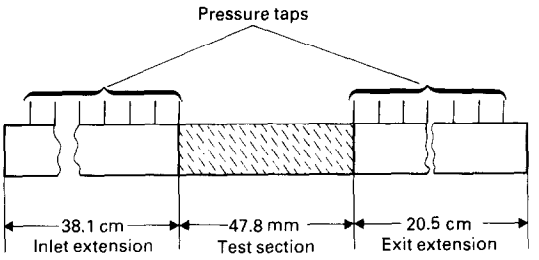

FIG. 3. Test section for pressure drop tests.

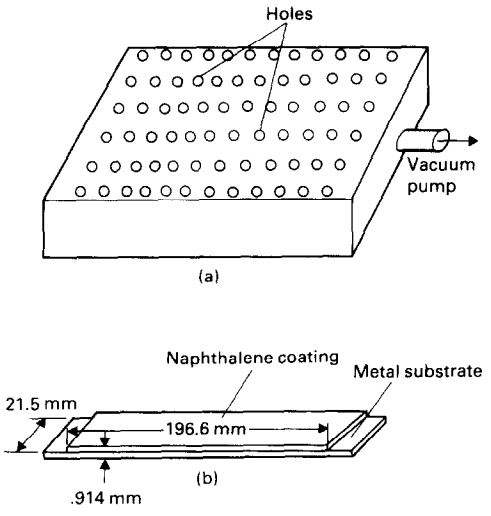

FIG. 4. Vacuum system for test plate making.

The vacuum system described above has two functions. One is to correct any possible warping of the plates on the platform before application of the coating naphthalene. The other is to hold the plates tight when the coating is machined.

In preparing the test plates, molten naphthalene is poured over the metal plates. The molten naphthalene spreads over them to form a free surface of naphthalene coating. When solidified, the thickness of the coating depends on the temperature of the molten naphthalene and the surface temperature of the metal strips.

The naphthalene coated on the metal plates is then machined to the required thickness, as shown in Fig. 4(b). The test plates prepared as per the above are stored in the supply air box [see (9) in Fig. 1] until they reach a thermal equilibrium. The test plates are then weighed with an analytical balance to determine the total mass, and installed in the test section. After a test run, the plates are removed and their mass is measured so as to determine the mass loss during the test run. Any extraneous mass transfer, which might occur during the installation and removal of the test plates, is determined to correct the mass loss. The run times are adjusted so that the mass loss is sufficient for the required accuracy of data; however, the change in the thickness of the naphthalene coating during a data run is small (less than 1.4×10^{-4} cm) for a lane of eight plates.

DATA REDUCTION OF HEAT TRANSFER RESULTS

The heat transfer coefficient is derived from the mass transfer coefficient as indicated earlier. The mass transfer coefficient h_m is evaluated from the corrected mass loss M and the duration time τ of the test run by the definition

$$h_m = M/(A_m \tau \Delta\rho_m) \tag{1}$$

where A_m is the transfer area of naphthalene sublimation and $\Delta\rho_m$ is the log mean concentration difference:

$$\Delta\rho_m = \frac{\rho_{ne} - \rho_{no}}{\ln[(\rho_{nw} - \rho_{no})/(\rho_{nw} - \rho_{ne})]}. \tag{2}$$

The quantity ρ_{nw} is the concentration of naphthalene vapor at the plate surface and was determined from the Sogin vapor pressure–temperature relationship [11]; ρ_{ne} is the concentration at the exit of the test section; ρ_{no} is the concentration at the entrance and is zero in the present work.

Since, however, the mass transfer surface area in the present model test section is much less than the total surface area for the flow, questions arise as to whether

the normal definition of the mass transfer coefficient h_m based on the log mean concentration defined above is valid, and whether the average mass transfer coefficient obtained from the forward-side and back-side coefficients represents the true average coefficient when the entire array participates in mass transfer.

In order to examine this, the mass transfer coefficient was calculated based on three concentration differences separately: the log mean, the average and the inlet. The coefficients obtained using the three methods were, however, identical in the present range of experiments.

Therefore, the heat transfer coefficient derived from the mass transfer coefficient obtained in the present work is considered to be identical to the heat transfer coefficient based on the log mean temperature. Also, a selected number of tests, as will be shown in the next section, confirm that the average heat transfer coefficient is identical even if both sides of the plates in the entire array participate in heat transfer.

The Sherwood number $N_{Sh,Dh}$ was evaluated from

$$N_{Sh,Dh} = h_m Dh/\mathscr{D} \tag{3}$$

Dh is the hydraulic diameter defined as per [1]

$$Dh = \frac{4A_c}{(A/L)} \tag{4}$$

where A_c = minimum cross-sectional flow area, A = total surface area for flow, and L = total array length in flow direction (NL_p).

The diffusion coefficient $\mathscr{D}$ is obtained from $N_{sc} = \nu/\mathscr{D}$ where $N_{sc} = 2.5$ [11] and ν is the kinetic viscosity of pure air.

The Reynolds number $N_{Re,Dh}$ is defined by

$$N_{Re,Dh} = \frac{\rho V_{max} Dh}{\mu} \tag{5}$$

where V_{max} = average flow velocity through A_c, μ = viscosity of air, and ρ = density of air.

Then, the Stanton number for mass transfer $(N_{St,Dh})_m$ is

$$(N_{St,Dh})_m = \frac{N_{Sh,Dh}}{N_{Re,Dh} N_{Sc}} \tag{6}$$

A_c is assumed to be unchanged with respect to the plate angle. The hydraulic diameter is fixed at $Dh = 52.81$ mm and the plate length to hydraulic diameter at $L_p/Dh = 0.407$ in the present work.

The Stanton number for heat transfer $N_{St,Dh}$ is

$$N_{St,Dh} = \frac{N_{Nu,Dh}}{N_{Re,Dh} N_{Pr}}. \tag{6'}$$

The Nusselt number $N_{Nu,Dh}$ is

$$N_{Nu,Dh} = h\,Dh/k \tag{3'}$$

where k is the thermal conductivity of air and h is the heat transfer coefficient.

The heat and mass transfer analogy implies the equality [10]

$$(N_{St,Dh})_m N_{Sc}^n = N_{St,Dh} N_{Pr}^n \tag{7}$$

where the power n is assumed to be 0.6.

HEAT TRANSFER RESULTS

Figures 5–8 show plots of $N_{Nu,Dh}$ vs $N_{Re,Dh}$ at plate angles of 20°, 25°, 30° and 35°, respectively.

Data shown by ○ are for the forward-side results, while those by ● are for the back side. Superimposed is the result (dotted line) obtained from the laminar flow theory for an ideal short duct corresponding to one plate pair [12, 13]. As expected, Nusselt numbers of the forward side are higher than those of the back side.

Figures 9–11 are the results of the cross plotting of the above results in $N_{Nu,Dh}$ vs θ with $N_{Re,Dh}$ as a parameter, on the forward side, the back side and the average of the two, respectively.

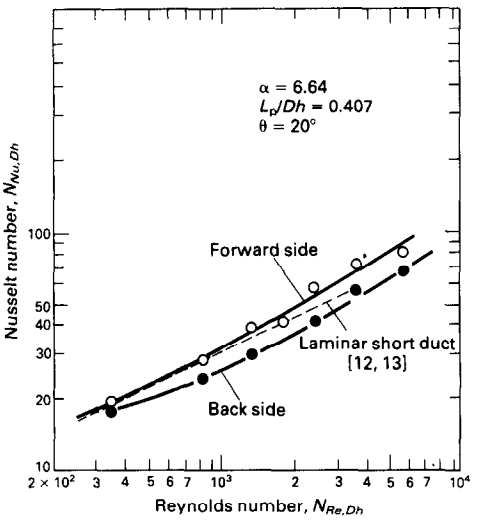

FIG. 5. Local heat transfer results at $\theta = 20°$: $N_{Nu,Dh}$ vs $N_{Re,Dh}$.

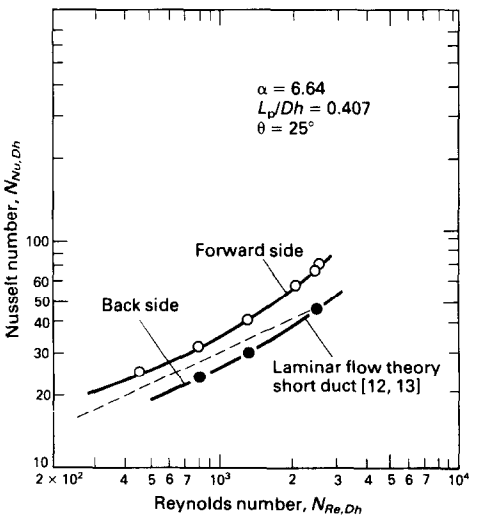

FIG. 6. Local heat transfer results at $\theta = 25°$: $N_{Nu,Dh}$ vs $N_{Re,Dh}$.

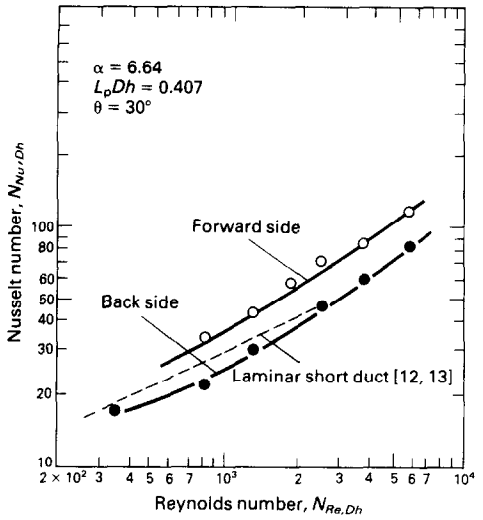

FIG. 7. Local heat transfer results at $\theta = 30°$: $N_{Nu,Dh}$ vs $N_{Re,Dh}$.

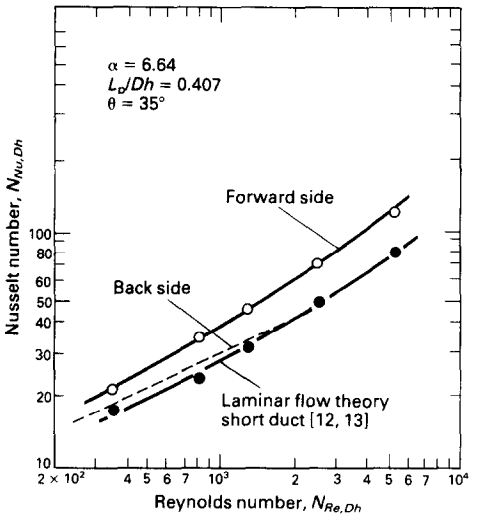

FIG. 8. Local heat transfer results at $\theta = 35°$: $N_{Nu,Dh}$ vs $N_{Re,Dh}$.

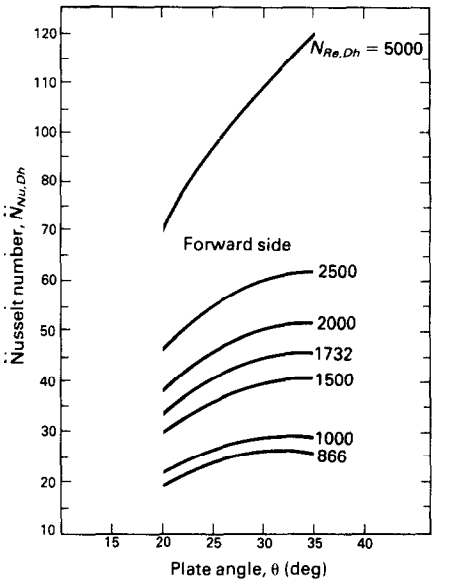

FIG. 9. Forward-side heat transfer results: $N_{Nu,Dh}$ vs θ.

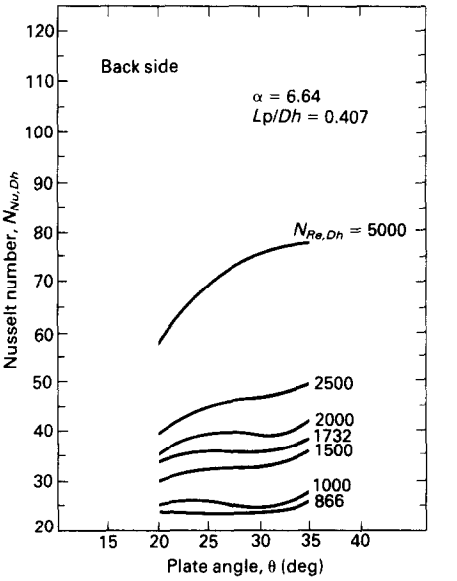

FIG. 10. Back-side heat transfer results: $N_{Nu,Dh}$ vs θ.

Figure 9 shows that the Nusselt number for the forward side continues to increase as θ increases ($\theta < 35°$) except at low $N_{Re,Dh}$. For $N_{Re,Dh} \leqslant 1500$, the Nusselt number tends to decrease at $\theta = 35°$ (a peak value at $\theta \approx 32.5°$). It is noted, however, that the variation in $N_{Nu,Dh}$ is small between $\theta = 30°$ and 35°.

Figure 10 shows a similar plot for the back side. It shows that the Nusselt number for the back side is insensitive to change in θ and fluctuates. At high $N_{Re,Dh}$, however, it increases as θ increases ($\theta \leqslant 35°$).

Since we are more interested in the average Nusselt number, Figs. 9 and 10 are combined to generate Fig. 11. It is seen that $N_{Nu,Dh}$ continues to increase as θ increases in the range of the experiments conducted. At $N_{Re,Dh} = 1732$, however, the gain in $N_{Nu,Dh}$ is only moderate; at $N_{Re,Dh} = 866$, the gain is minute.

To confirm the accuracy of the data, a separate set of data at $\theta = 35°$ have been obtained with the entire array of plates, each having naphthalene coating on both sides and compared with the data of Fig. 11. The results shown in Fig. 12 confirm the accuracy of the data.

Comparison with the literature and data of louvered fin heat exchanger

An objective of the present work is to characterize the heat transfer performance of a plate array—a variation of a continuous surface segmented transversely to the flow direction. Therefore, it is now in order that the results of the present work be compared with those of the unsegmented continuous surface in the literature. To this end, the prior work on laminar flow [12, 13] and Latzko's work [14] on

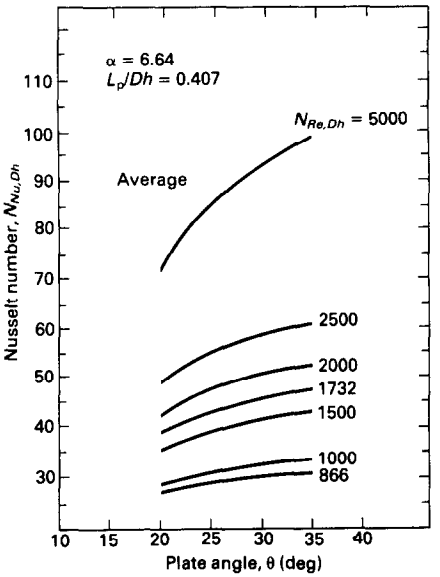

FIG. 11. Average heat transfer results: $N_{Nu,Dh}$ vs θ.

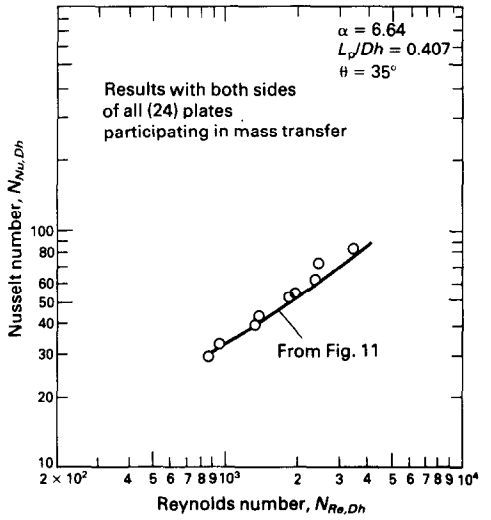

FIG. 12. Average heat transfer results (both sides of all plates participating in mass transfer).

developing turbulent flow of a rectangular duct having an aspect ratio of $\alpha = 6.65$ and a duct length-to-hydraulic diameter ratio of $L/Dh = 3.256$ (eight times L_p/Dh) are presented in Fig. 13 along with the present results of $\theta = 30°$. It is seen that the $N_{Nu,Dh}$ of the plane array exceeds that of the continuous long duct by a factor of 2.75–4. The heat exchanger, which is most relevant to the present results, is an automotive radiator equipped with louvered fins. For that reason, data from tests of a radiator having geometrical features ($\alpha = 7.4$, $L_p/Dh = 0.4$, $\theta = 29°$) similar to those of the plate array are superimposed in Fig. 13.

Although a deviation between the radiator results and the present data is expected, since the two systems have differences in details of geometrical features, the magnitude of the difference in $N_{Nu,Dh}$ (2:1) requires an

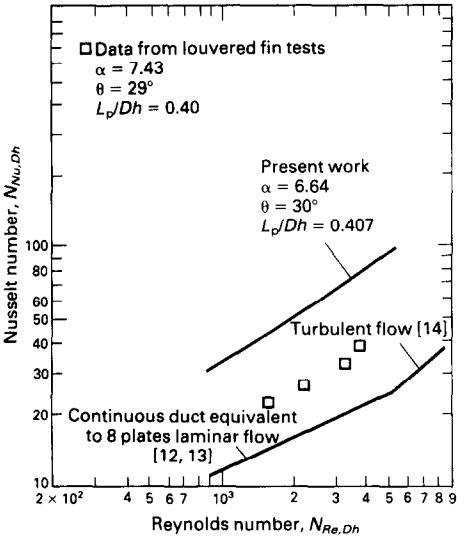

FIG. 13. Comparison with louvered fin test data: $N_{Nu,Dh}$ vs $N_{Re,Dh}$.

analysis of the radiator fin geometry and the test section. The following features are the main differences:

(1) While the louvers do not span the entire space between the two flat tubes in the radiator as shown in Fig. 14, the model simulates the louvered fins spanning the entire span.
(2) The radiator has two louver orientations in the louver array. Over the forward portion of the fin, the louvers subtend an angle θ with respect to the air flow; and over the rear portion of the fin, this angle becomes $\pi - \theta$. Such a change in the orientation requires a transition section. On the other hand, all plates (eight in number) used for the experiments are in forward orientation against the air flow.

The significantly large difference between the radiator test results and the present data is an incentive for further investigation of the contribution of the individual parameters discussed above.

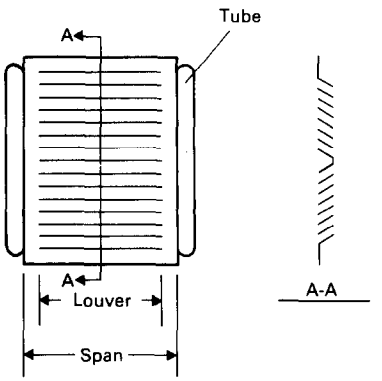

FIG. 14. Fin configuration of louvered fin radiator.

PRESSURE DROP RESULTS

The total pressure drop ΔP_T through the duct with the plate array can be broken down into three components which are the pressure drop due to friction ΔP_f and that due to inertia losses through the plate array ΔP_p and the entrance/exit losses ΔP_e, respectively

$$\Delta P_T = \Delta P_N + \Delta P_e \quad (8)$$

where $\Delta P_N = \Delta P_f + \Delta P_p$.

Figure 15 is a typical pressure drop pattern along the duct (the plate angle = 20°, the average velocity = 4531 m h^{-1}) when the plates are aligned at a positive angle to the air flow. It is seen that the pressure drop data fall on a straight line in the upstream section, and that near the trailing edge there is substantial pressure depression. However, the pressure depression is recovered along the downstream duct and data fall on a straight line again. Without the plate array, the two straight lines would be colinear. Thus, a net pressure drop ΔP_N of the array is the difference offset by the two lines [between (A) and (B)].

However, the total pressure drop ΔP_T varies depending on where the duct exit ends in Fig. 15. For instance, if the duct terminates at the end of the array ΔP_e, and hence ΔP_T, becomes its maximum.

The pressure drop has also been measured with the plates aligned at a negative angle to the air flow. An example of the test results is shown in Fig. 16 when the plate angle is 25° and the average velocity is 4572 m h^{-1}. A small pressure increase, rather than the pressure depression, is observed near the trailing edges of the plate array. The increase in pressure, however, is not pressure recovery but due in part to stagnation pressure. Note that the net pressure drop ΔP_N is

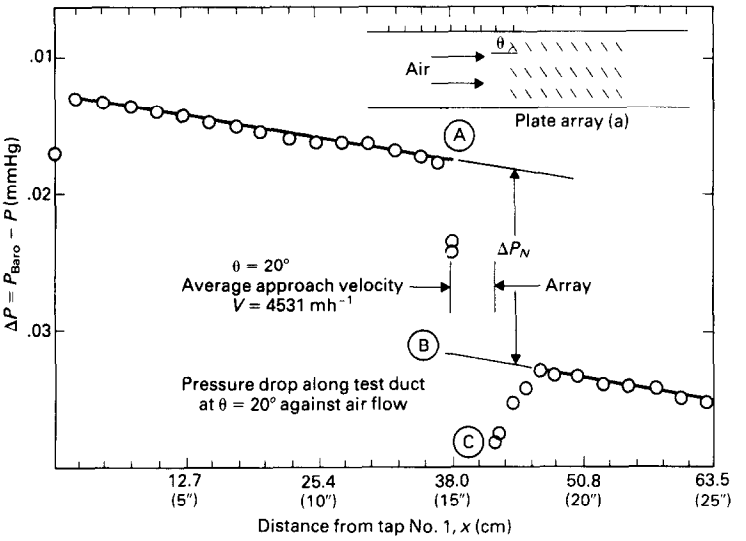

FIG. 15. Pressure variation in duct with plate array (a).

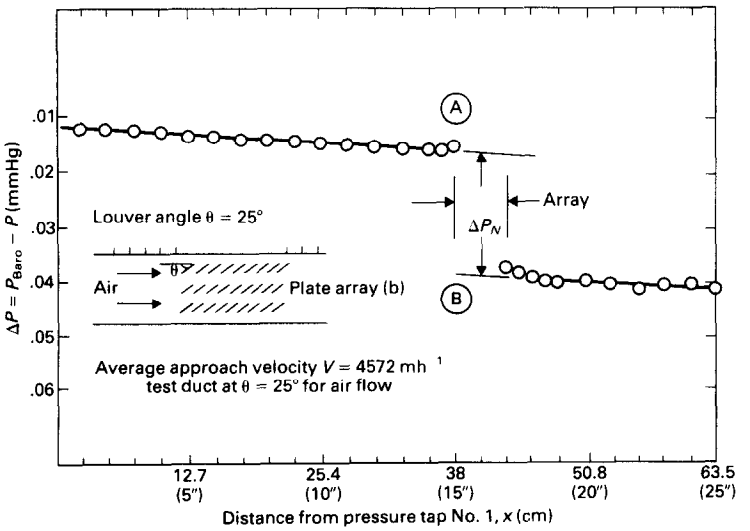

FIG. 16. Pressure variation in duct with plate array (b).

identical regardless of whether the plates are oriented for the air flow or against it.

Each of the above pressure drop components can be expressed by

$$\Delta P_f = \tfrac{1}{2}\rho V_{max}^2 f\left(\frac{L_p}{Dh}\right)N \quad (9)$$

$$\Delta P_p = \tfrac{1}{2}\rho V_{max}^2 K_p N \quad (10)$$

$$\Delta P_e = \tfrac{1}{2}\rho V_{max}^2 K_e. \quad (11)$$

Hence

$$\Delta P_N = \tfrac{1}{2}\rho V_{max}^2 N[f(L_p/Dh)+K_p]. \quad (12)$$

The pressure coefficients K_p (and also K_e) are due to inertia losses and independent of Reynolds number $N_{Re,Dh}$ for a given θ; however, $f(L_p/Dh)$ is a function of both $N_{Re,Dh}$ and L_p/Dh.

Friction coefficient, f

From measurements of the pressure variation in developing flow through the upstream duct, the friction coefficient f has been determined and shown in Fig. 17. As shown in the figure, the results are quite close to the Blasius correlation for a fully developed flow in a smooth pipe having a diameter D [14]. Assuming that a similar relationship would hold through the plate array, the first term in equation (12) is estimated to be negligibly small compared with the second term as per ref. [8].

Pressure coefficient per row K_p

Pressure drop data obtained as per the procedure outlined in Figs. 15 or 16 are plotted in terms of the bracketed value of equation (12) $[f(L_p/Dh)+K_p]$ vs Reynolds number $N_{Re,Dh}$, with the plate angle θ as the parameter, in Fig. 18. It is seen that $[f(L_p/Dh)+K_p]$ is constant for all plate angles. This suggests that $f(L_p/Dh) \ll K_p$ as expected and that the pressure drop penalty would be significantly high.

Exit loss coefficient K_e

As indicated earlier, the exit loss varies with the degree of pressure recovery in the downstream. It can become a significant portion of the total pressure drop. To estimate this upper limit of its impact, the maximum exit loss coefficient $(K_e)_{max}$ is determined at each plate angle. The results are shown in Fig. 19; also superimposed is the plot of K_p. It is seen that $(K_e)_{max}$ reaches close to unity at $\theta \approx 25°$, and that the number of plate rows must be large for the effect of the exit loss to be small.

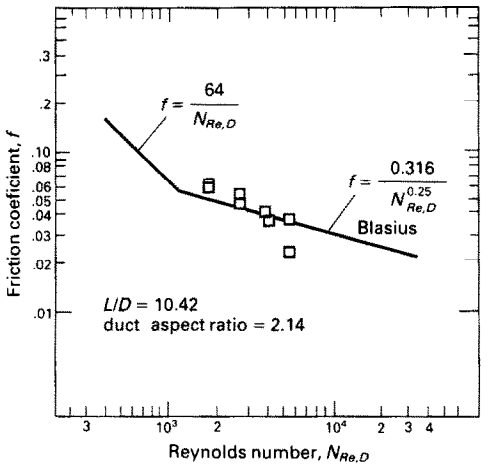

FIG. 17. Friction coefficient f.

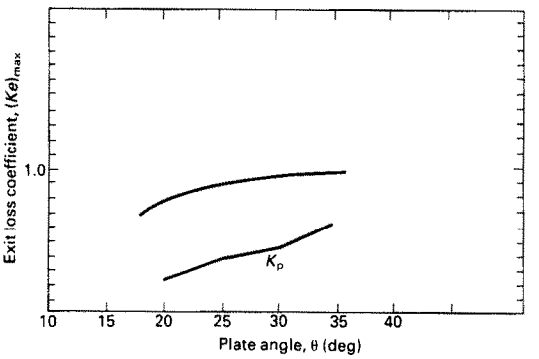

FIG. 19. Average maximum exit loss coefficient $[(K_e)_{max}]_{ave}$.

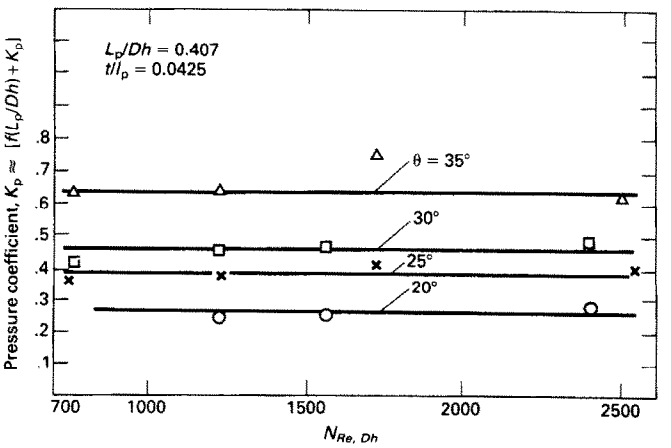

FIG. 18. Pressure coefficient vs Reynolds number.

PERFORMANCE EVALUATION

The preceding sections of the paper demonstrated that an array of short plates aligned at angles to the flow direction has an advantage over a long plate duct in heat transfer but is accompanied by a pressure drop penalty. Now the two systems are evaluated on a constraint common to both. One convenient constraint is the fixed pumping power PP to operate them. The Nusselt number ratio $N_{Nu,Dh}/(N_{Nu,Dh})_{oo}$ will be used as the criterion for the heat transfer performance where $(N_{Nu,Dh})_{oo}$ is the Nusselt number for the long continuous plate duct.

For equal pumping power, it can be shown readily that the following condition must be met:

$$N_{Re,Dh}^3 K_p = (N_{Re,Dh})_{oo}^3 f \frac{L_p}{Dh}. \quad (13)$$

Let us assume that f follows the Blasius correlation. For given plate angle and Reynolds number $N_{Re,Dh}$, the Reynolds number of the long duct $(N_{Re,Dh})_{oo}$ that satisfied equation (13) can be computed. The Nusselt number ratio is then obtained from Figs. 11 and 13. The computed results are plotted in Fig. 20. It is seen that the improvement in the $N_{Nu,Dh}$ of the segmented plate array is more pronounced at low Reynolds numbers than at high Reynolds numbers, ranging from factors of 1.2 to 1.72. It is also seen that an optimum plate angle appears to exist near $\theta = 30°$.

CONCLUDING REMARKS

The present experiments have demonstrated that the heat (mass) transfer from an array of plates aligned at angles to the streamwise direction brings about a significant increase in the Nusselt number compared with the unsegmented continuous plate. A comparison with the developing flow regime showed the Nusselt number increase can be as high as a factor of four. However, the pressure drop increase is also high due to the presence of the segmented plates. Still, the Nusselt number increase for the fixed pumping power is shown to be a factor of nearly two.

The present experiments have also revealed that there exists an optimum plate angle.

A significant difference in the Nusselt number between the present work and the test data obtained from a louvered fin radiator provides an incentive for further investigation on other geometric parameters which differ from those of the ideal configuration that the present investigation dealt with.

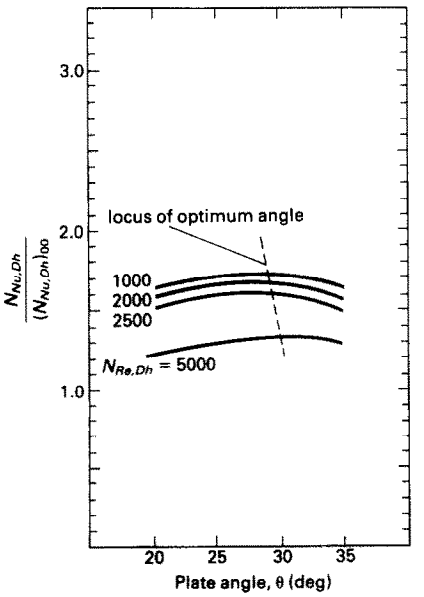

FIG. 20. Optimum plate angle.

Acknowledgement—The author expresses his thanks to Long Manufacturing, Ltd., Oakville, Canada, who kindly provided data.

REFERENCES

1. W. M. Kays and A. L. London, *Compact Heat Exchangers*, 2nd edn. McGraw-Hill, New York (1964).
2. R. K. Shah, Perforated heat exchange surfaces. Part 2—Heat transfer and flow friction characteristics, ASME Paper 75-WA/HT-9 (1975).
3. R. K. Shah and A. L. London, Offset rectangular plate-fin surfaces—heat transfer and flow friction characteristics, *J. Engng Pwr* **90**, 218–228 (1968).
4. A. R. Wieting, Empirical correlation for heat transfer and flow friction characteristics of rectangular offset-fin plate-fin heat exchangers, *J. Heat Transfer* **97**, 488–490 (1975).
5. F. N. Beauvais, An aerodynamic look at automotive radiators, Mid-year SAE meeting (1962).
6. M. C. Smith, Performance analysis and model experiments for louvered fin evaporator core development, SAE Paper 720078.
7. N. Cur and E. M. Sparrow, Experiments on heat transfer and pressure drop for a pair of colinear, interrupted plates aligned with the flow, *Int. J. Heat Mass Transfer* **21**, 1069–1080 (1978).
8. E. M. Sparrow and A. Hajiloo, Measurements of heat transfer and pressure drop for an array of staggered plates aligned parallel to an air flow, *J. Heat Transfer* **102**, 427–432 (1980).
9. S. V. Patankar, C. H. Liu and E. M. Sparrow, Fully developed flow and heat transfer in ducts having streamwise-periodic variations of cross-sectional area, *J. Heat Transfer* **99**, 180–186 (1977).
10. E. R. G. Eckert and R. M. Drake, Jr., *Heat and Mass Transfer*. McGraw-Hill, New York (1959).
11. H. H. Sogin, Sublimation from disks to air streams flowing normal to their surfaces, *Trans. Am. Soc. mech. Engrs* **80**, 66–71 (1958).
12. R. K. Shah and A. L. London, *Laminar Flow Forced Convection in Ducts, Advances in Heat Transfer*, Supplement 1. Academic Press, New York (1978).
13. W. E. Mercer *et al.*, Laminar forced convection in the entrance region between parallel flat plates, *J. Heat Transfer* **89**, 251–257 (1967).
14. L. E. Sissom and D. R. Pitts, *Elements of Transport Phenomena*. McGraw-Hill, New York (1972).

CARACTERISTIQUES DU TRANSFERT THERMIQUE ET DE PERTE DE CHARGE D'UNE RANGEE DE PLAQUES INCLINEES SUR L'ECOULEMENT DANS UN CANAL RECTANGULAIRE

Résumé—On étudie expérimentalement, dans le domaine de nombre de Reynolds entre 300 et 5000, le transfert de chaleur et la perte de charge pour une rangée de plaques alignées avec des angles $\theta = 20$–$35°$ sur la direction de l'écoulement d'air dans un canal rectangulaire droit. Les coefficients de convection thermique sur les deux faces des plaques ont été déterminés séparément et le coefficient moyen entre les deux approche de près la théorie laminaire de conduite courte, aux faibles nombres de Reynolds ($N_{Re,Dh} \leqq 1200$) et il est presque indépendant de l'angle d'alignement par rapport à la direction de l'air. Aux plus grands nombres de Reynolds ($N_{Re,Dh} \geqq 1500$) le coefficient moyen s'écarte significativement de la théorie. Les mesures de perte de charge à travers la rangée de plaques montre que le coefficient K_p est une fonction seulement de l'angle de la plaque et indépendant du nombre $N_{Re,Dh}$.

WÄRMEÜBERGANG UND DRUCKVERLUST AN EINER ZUR STRÖMUNG IN EINEM RECHTECKKANAL UNTER VERSCHIEDENEN WINKELN ANGESTELLTEN PLATTENREIHE

Zusammenfassung—Wärmeübergang und Druckverlust an einer Plattenreihe, die mit verschiedenen Winkeln von $\theta = 20$–$35°$ zur Richtung des Luftstroms in einem geraden Rechteckkanal angestellt ist, wurde bei Reynolds-Zahlen zwischen 350 und 5000 experimentell untersucht. Die Wärmeübergangskoeffizienten an Vorder- und Rückseite der Platten wurden getrennt bestimmt. Ihr Mittelwert kommt der Theorie für kurze Kanäle und kleine Reynolds-Zahlen ($N_{Re,Dh} \leqslant 1200$) sehr nahe und ist fast unabhängig vom Anstellwinkel gegen die Luftströmungsrichtung. Jedoch weicht der mittlere Koeffizient bei höheren Reynolds-Zahlen ($N_{Re,Dh} \geqslant 1500$) wesentlich von der Theorie ab. Die Druckverlustmessungen längs der Plattenreihe zeigen, daß der Koeffizient K_p (je Reihe in Strömungsrichtung) nur eine Funktion des Plattenanstellwinkels ist; von der Reynolds-Zahl $N_{Re,Dh}$ ist er unabhängig.

ХАРАКТЕРИСТИКИ ТЕПЛООБМЕНА И ПЕРЕПАДА ДАВЛЕНИЯ НА РЕШЕТКЕ ИЗ ПЛАСТИН, РАСПОЛОЖЕННЫХ ПОД УГЛАМИ К ПОТОКУ В ПРЯМОУГОЛЬНОМ КАНАЛЕ

Аннотация—Проведено экспериментальное исследование характеристик теплообмена и перепада давления на решетке из пластин, расположенных под углами $\theta = 20$–$35°$ к потоку воздуха в прямоугольном канале при $350 \leq Re \leq 5000$. Коэффициенты теплообмена для обеих сторон пластин определяются раздельно, а их среднее значение хорошо аппроксимируется с помощью теории ламинарного течения в коротком канале при малых значениях числа Рейнольдса ($N_{Re,Dh} \leq 1200$) и почти не зависит от угла расположения пластин относительно направления потока воздуха. Однако, при более высоких значениях числа Рейнольдса ($N_{Re,Dh} \geq 1500$) средняя величина коэффициента значительно отклоняется от теоретического значения. Измерения перепада давления вдоль пластин показали, что коэффициент K_p, рассчитанный вдоль решетки вниз по потоку на один ряд, зависит только от угла наклона и не зависит от числа Рейнольдса $N_{Re,Dh}$.